Preliminary study of a customised total knee implant with musculoskeletal and dynamic squatting simulation

Article (Accepted Version)

Preliminary study of a customised total knee implant with musculoskeletal and dynamic squatting simulation

Linjie Wang[1], Chang Jiang Wang[1]

[1]Department of Engineering and Design, University of Sussex, Falmer, Brighton, BN1 9RH, UK

Abstract

Customised total knee replacement could be the future therapy for knee joint osteoarthritis. A preliminary design of a customised total knee implant (CTKI) based on knee anatomy was studied in this paper. To evaluate its biomechanical performance, a dynamic finite element model based on the Oxford knee rig was created to simulate a squatting motion. Unlike previous research, this dynamic model was simulated with patient-specific muscle and joint loads that were calculated from an OpenSim musculoskeletal model. The dynamic response of the CTKI was simulated under three cruciate ligament scenarios: both cruciate ligaments retained, only anterior cruciate removed and both cruciate ligaments removed. In addition, an off-the-shelf symmetric total knee implant (STKI) with retained cruciate ligaments was simulated for comparison analysis. The CTKI with both cruciate ligaments retained showed larger ranges of femoral external rotation and posterior translation than the STKI. The motion of the CTKI was also in good agreement with a healthy knee. There were no big differences in the tibiofemoral compressive forces in the CTKI model under the three scenarios. These forces were generally consistent with other experimental and simulation results. However, the CTKI design resulted in larger tibiofemoral compressive force than the STKI after 50° knee flexion, which was caused by the larger tibiofemoral relative motion.

Keywords: customised total knee implant, musculoskeletal model, dynamic tibiofemoral compressive forces, tibiofemoral relative motions, comparison analysis

Authors:

Linjie Wang

lw302@sussex.ac.uk

Affiliation: Department of Engineering and Design, University of Sussex

Address: Richmond building 3A4, University of Sussex, Falmer, Brighton, BN1 9QT

Chang Jiang Wang

C.J.Wang@sussex.ac.uk

Affiliation: Department of Engineering and Design, University of Sussex

Address: Richmond building 3A8, University of Sussex, Falmer, Brighton, BN1 9QT

Corresponding author:

Linjie Wang

lw302@sussex.ac.uk

Affiliation: Department of Engineering and Design, University of Sussex

Address: Richmond building 3A4, University of Sussex, Falmer, Brighton, BN1 9QT

1. Introduction

Total knee replacement has been used to treat severe knee arthritis with various implant designs for several decades. However, patients often report post-operative dissatisfaction[1–5]. The two leading reasons for this are the residual pain caused by the overhang of total knee implants (TKIs) on bones, and the knee function limitation which may be associated with the conformity between the femoral and tibial components.

Currently, most off-the-shelf TKIs are designed with two parallel arc-shaped condylar surfaces. The sagittal condylar contour of the femoral component is normally simplified as single, dual or gradually changing multi-radii. Bonnefoy-Mazure et al.[6] and Rahman et al.[7] studied the kinematics of knees that had been replaced with off-the-shelf designs 3 and 12 months post-surgery respectively. Both studies concluded that knee function was not fully restored in terms of knee range of motion. Walker et al.[8] demonstrated that asymmetric design of an implant was able to produce the asymmetries that occur in the motion of the native knee. Patil et al.[9] compared a customised knee implant from ConforMIS with a standard off-the-shelf cruciate retaining TKI from DePuy based on the Oxford knee rig (OKR) and found that patient-specific designed knee implants could produce kinematics that more closely resemble normal knee kinematics than standard off-the-shelf implants. However, in their experiments, the effect of coordinated muscle forces was neglected, and close-to-physiological hip and ankle joint forces were not applied. In fact, these two problems are common in assessment of TKI performance by either computer simulation[10–14] or in-vitro experiment[15–17] based on the OKR[18, 19] or the Kansas Knee Simulator (KKS) [20, 21]. In reality, muscle forces do play an important role in joint motion because medium to high quadriceps, hamstrings, and gastrocnemius activities are produced during squatting.[22]

One of the objectives of the research reported in this paper is to create a customised total knee implant (CTKI) based on the anatomy of a specific patient for conducting comparison analysis. Another is to create a computer finite element (FE) knee simulation model with reference to the OKR and KKS, to evaluate the dynamic response of the knee implants. Unlike previous research, the model in this paper will include the effect of patient-specific muscle and ground reaction forces during squatting. By comparing the kinematic and kinetic results between the CTKI and an off-the-shelf symmetric total knee implant (STKI), it is expected that this study can determine whether the CTKI is able to improve patient knee function during squatting. By incorporating lower limb muscle forces and ground reaction forces into the FE models, it could help make the performance assessments on TKIs closer to physical and physiological circumstances.

2. Material and Methods

2.1 Modelling of customised total knee implant

Through feature point identification, least squares elliptical curve fitting and surface regeneration, a femoral implant (Fig. 1(a)) was created from a 3D patient-specific knee joint model. This model was built in 3D Slicer[23] (available from http://www.slicer.org,) from CT images of the subject model JW (mass 66.7 kg, height 1.68m) on the website (https://simtk.org/projects/kneeloads) for the 4th Grand Challenge Competition to Predict In Vivo Knee Loads.[24] The detailed design process for the customised implant is explained in the Appendix. The right knee joint of the subject was replaced with a total knee implant in the 4th Grand Challenge Competition. However, CT images for creation of the model were only available for the left knee joint. Thus the exact STKI used in the Grand Challenge Competition could not be used for the modelling in this study. It was also felt preferable not to compare the CTKI with a specific implant from any manufacturer. The STKI model was therefore scaled up from the CAD model of a knee implant, which had been previously created based on the DePuy PFC Sigma model[25], to align its AP dimension with the patient's distal femur.[26] In contrast to the complete fit between the femoral bone and the asymmetric and anatomic-shaped femoral implant shown in Fig. 1(a), several overhangs/underhangs between the STKI model[25] and the bone can be seen in Fig. 1(b). Meanwhile, the revolute centre of the femoral component was placed coincident with the femur distal centre which was the middle point between two epicondyle points.

Fig. 1

In terms of the tibial implant modelling, because the information about the subject's menisci is not available, the tibial bearing surface was created based on the shape of the femoral component condyles by defining an elliptical cutting guide track in the longitudinal direction and two quadratic curves in the transverse direction on each condyle (Fig. 2(a)). The detailed design process for the tibial bearing surface is also explained in the Appendix. A scaled tibial implant from the DePuy PFC Sigma model[25] is shown in Fig. 2(b) for comparison between its symmetric structure and the asymmetric characteristic of the CTKI. The responses of both the CTKI and the STKI were simulated under squatting motion. Their kinematic and kinetic results were compared to identify any difference in knee function between the two implants.

In contrast to the off-the-shelf STKI, the CTKI in this paper is still only in the concept design stage without many features. The CTKI model shown in Fig. 2(a) only considered the tibiofemoral contact surfaces without other implant details, such as the fenestrations on the tibial implant for retaining both anterior and posterior ligaments.

Fig. 2

2.2 Musculoskeletal model for calculating muscle forces and joint reaction forces

To be able to simulate and predict the response of the CTKI and STKI under close-to-physiological conditions, lower limb muscles forces around the knee and ankle joints are needed. These muscle forces and ankle joint reaction loads (Fig. 3) were obtained from a squatting simulation of a patient-specific musculoskeletal model. The musculoskeletal model was built in OpenSim by scaling a generic model 2392 based on the experimental data of Subject JW[24]. Inverse kinematics analysis was conducted to acquire the motion of squatting. By incorporating the measured ground reaction forces into the analysis of the residual reduction algorithm (RRA) in which the nonphysical compensatory residual loads are assumed and appliedon the subject pelvis, the subject kinematics including the hip flexion rotation could be adjusted to be more dynamically consistent with the ground reaction forces. The maximum and root mean square of the residual loads on the pelvis centre were evaluated and found to be within the ranges of evaluation thresholds specified in the online OpenSim Documentation for 'Getting Started with RRA'. Subsequently, the adjusted kinematic results were used as the desired motion in the static optimization analysis for tracking to calculate the muscle forces using the inbuilt optimization algorithm. Finally, using the joint reaction analysis in OpenSim, the ankle joint loads acting on the tibia bone were calculated and could be imported together with muscle forces and hip flexion angles into the dynamic Finite Element (FE) model for assessing and comparing the performance of total knee implants. This dynamic FE model is described in the following section. The subject's left leg mass and mass centres, which were scaled through the static pose markers, are listed in Table 1; they were applied in the FE model as lumped masses.

Table 1

Fig. 3

2.3 Dynamic finite element modelling based on the Oxford and Kansas knee rigs

Forward dynamic analysis in OpenSim with meshed articulation surfaces of femoral and tibial components was conducted initially. However, this resulted in very high knee contact forces or solution divergence due to excessive penetration between the articulation surfaces. This is because OpenSim uses an elastic foundation algorithm rather than a penalty method for contact force calculation. The relative motion of the resurfaced tibiofemoral joint cannot then be adjusted under the muscle and joint reaction forces derived from the motion of

the pre-resurfaced knee joint. Therefore, a dynamic FE model was created with reference to the Oxford and Kansas rigs to predict the dynamic response of the CTKI to the leg muscle and ankle joint forces. The knee implant was placed in alignment with the mechanical axis which is perpendicular to the joint line so that the vertical joint load could be evenly distributed through the two condylar surfaces while standing. Three translational and two rotational loads from OpenSim were applied at the ankle joint in this FE model, and a load that was a function of flexion angle versus time that was also obtained from OpenSim was applied at the hip joint. The translational degrees of freedom (DOFs) of the hip were fixed to the ground which is similar to that in the knee simulator developed by Verstraete and Victor[16]. The STKI was also analysed under the same method and boundary conditions for comparison analysis. Due to limited functionality in ANSYS software, control loop or feedback was not used in the dynamic FE simulations.

Fig. 4

2.3.1 Joint definitions and boundary conditions

ANSYS joint elements (MPC184) were used to simulate hip and ankle joints of the subject JW. The hip joint was specified to have two rotational DOFs that represent flexion-extension and adduction-abduction motions, while the ankle joint has all six DOFs (Fig. 4(a)). The locations of these two joints were determined from the OpenSim model.

2.3.2 Ligament and musculotendon models

The two collateral ligaments (Fig. 4(b)): lateral collateral ligament (LCL) and medial collateral ligament (MCL) and the two cruciate ligaments (Fig. 4(c)): anterior cruciate ligament (ACL) and posterior cruciate ligament (PCL) were modelled as nonlinear springs with appropriate insertion points on the femur and tibia respectively, while the patellar ligament (PL) was simulated as a linear spring due to the lack of relevant data about it in the literature. Based on a reported stiffness for the PL of 210±66 N/mm in the literature[27], the PL was split into three bundles each with a spring stiffness of 70 N/mm. All the ligaments except the PL in this model were applied with preloads as reported in the literature[13, 28, 29]. The force-displacement curve for the ligaments was described by Eqs. (1) and (2). The parameter kk is the stiffness parameter, ll_0, the zero-load length and ε_{al}, the spring parameter of 0.03.[30] In this study, three different scenarios of cruciate ligament treatment, namely both ACL and PCL retained, only ACL removed and both ACL and PCL removed, during surgery were simulated on the CTKI model from the knee extension posture to the maximum knee flexion angle during a squat. Forces and elongations of all the ligaments were extracted for analysis. The STKI model was only simulated with both cruciate ligaments

retained, because the result of CTKI with both cruciate ligaments retained was much closer to healthy knees in this study.

$$FF = \begin{cases} 1 & 0 \le \varepsilon \le 2\varepsilon_l \\ k\varepsilon^2/\varepsilon_l & \\ k(\varepsilon - \varepsilon_l) & \varepsilon > 2\varepsilon_l \\ 0 & \varepsilon < 0 \end{cases} \quad (1)$$

$$\varepsilon = (l - l_0)/l_0 \quad (2)$$

Table 2

Fig. 5

The quadriceps muscles (Fig. 4(d)) were split into four bundles with three muscle insertion points on the femur and one on the pelvis. Because only segments of the femur and tibia from 11 to 15 cm above and below the joint line could be built from the accessible CT data, the locations of the four muscle insertion points on either the upper femur or the pelvis were determined from the OpenSim musculoskeletal model. All the muscle insertion points on the femur were rigidly connected to the point in the hip joint origin that acted as pilot node through the multipoint constraint (MPC) technology (Fig. 5), while other muscle insertion points on the tibia were connected to the pilot node in the ankle joint origin. Since the pelvis and calcaneus to which some muscles around the knee joint were attached were not included in this FE model, the insertion points on the pelvis or calcaneus were built as translational joints with the ability to rotate around a spherical joint (Fig. 5). This ensured that the time-varying muscle forces would pass through the insertion points on the pelvis or the calcaneus and not produce any extra loads on the hip or the ankle joint. It would also mean that the direction of the forces during the knee flexion would be self-adjusting. Each node at a muscle insertion point was connected with a translational joint element by defining a spherical joint element. The node was then rigidly connected to the pilot node in either the hip joint or the ankle joint thorough a weld joint element (Fig. 5).

One end of an actuator element (Fig. 5), LINK11, was connected to four quadriceps muscle bundles. This actuator element supports force-time functions and is able to apply a time-varying load along the axial direction of the muscle bundle. At the other end of the actuator element was a spherical joint node. The femoral and tibial bones were removed from the dynamic analysis to reduce the computational cost.

2.3.3 Measurement of relative motions between two objects

A rotation matrix was applied to calculate the relative rotations or Euler angles between the femoral and tibial

local coordinate systems (CS) which were built through four nodes and their rigid links within each component. Relative rigid translations could be calculated from the distances between the femoral and tibial CS origins. Both rotations and translations were expressed in the tibial CS as well as two condylar compressive forces in body weight (BW) in the vertical direction of the tibial CS.

2.3.4 Materials and model verification

Material properties are listed in Table 3. The ultra-high molecular weight polyethylene (UHMWPE) is a common material for tibial inserts. The femoral implant is made of Cobalt-Chrome alloy. Titanium alloy is used for modelling the tibial tray of 3 mm thickness[25] in the simulations. No relative motion was assumed between the tibial insert and tibial tray. The patellar bone was assumed to have cortical bone properties.

Table 3

In terms of the control load steps in the ANSYS iteration solver, the maximum time-step was set to be 0.01 seconds and the minimum 0.001 seconds. Automatic time stepping was also activated. These settings ensured that all the modes and responses of interest would be predicted.

Contact pairs of the tibiofemoral and patellofemoral joints were defined using the ANSYS default contact setting. The element size of the contact surfaces of these two joints was 2 mm. The element size for volume mesh was 4 mm. Mesh sensitivity was studied; further mesh refinement resulted in less than 5% change in the predicted peak contact pressures.

3. Results

Fig. 6

The relative motions between the femoral and tibial components are presented in Fig. 6. It is worth noting that, in Fig. 6(a), the results of femoral external rotation in relation to the tibia for the CTKI models with all ligament scenarios were in good agreement with that of five healthy males in-vivo measured by Murakami et al.[31] through fluoroscopic study. However, for the anteroposterior translation in Fig. 6(b), only the motion of the CTKI with both cruciate ligaments retained was close to that of healthy knees.

The STKI model simulated under the same conditions as the CTKI also showed constant femoral rotation but with a smaller ROM and paradoxical internal rotation. For its posterior translational motion, the femoral component slid 5 mm anteriorly on the tibial component until 30° knee flexion, and then moved posteriorly by 7

mm until the maximum knee flexion angle.

As for the remaining DOFs of the knee joint, the CTKI model did not show significant differences in the adduction-abduction rotation and superior-inferior translation under the three cruciate ligaments scenarios. However, for the medial-lateral translation, the model with both cruciate ligaments retained showed larger medial but smaller lateral translations. The femoral medial-lateral translation in the STKI in Fig. 6(c) remained constant. In Fig. 6(d), the STKI model resulted in a different trend for femoral adduction rotation to that of the CTKI. In Fig. 6(e), the femoral superior translation in the STKI model was smaller than that of the CTKI.

Fig. 7

The tibiofemoral (TF) compressive forces are shown in Fig. 7. There are no large differences among the three scenarios, though the joint forces of the model with retained cruciate ligaments were slightly larger than that of the other two scenarios because the ACL tension force was applied to the tibiofemoral articular surface (Fig. 7(a)). The simulated knee forces in this paper were quite close to the experimental results (cyan dash lines) obtained by Stylianou et al.[32] until 60° knee flexion. Above that flexion level, the results tended to be much closer to experimental data (black dash lines) reported by Taylor et al.[33]. The results in this paper were also generally consistent with the results calculated by Bersini et al.[34]. The results for the STKI are shown as black dotted lines in Fig. 7. Above 50° knee flexion, the STKI resulted in smaller tibiofemoral compressive forces than the CTKI. From 58° knee flexion, the compressive force for the STKI started to reduce till 75° knee flexion when it increased slightly again.

As for the compressive forces on the medial and lateral condyles, the medial condylar force in the CTKI model was larger than that in the STKI model, while the lateral condylar force in the CTKI model was smaller than that in the STKI model. With the increase of knee flexion angle, the medial condyle in the CTKI model was subjected to larger load than the lateral condyle. In the STKI model, although the medial condylar force was larger than the lateral side above 40° knee flexion, its medial-lateral load ratio was smaller than that of the CTKI.

The results for ligament forces in the CTKI model are shown in Fig. 8. The MCLs were subjected to larger loads and longer elongations compared to the LCLs due to the larger initial strains in the MCLs (Figs. 8(a) and 8(b)). Both aLCL and mLCL were relaxed for most of time until 50° knee flexion for mLCL and 60° for aLCL (Figs. 8(c) and 8(d)). The patellar ligaments were not susceptible to the different cruciate ligament scenarios (Fig. 8(e) and Fig. 8(f)). In Fig. 8(g) and Fig. 8(h), the ACLs were extended until 3° knee flexion for the pACL and 48°

for the aACL and then shortened till 50° and 76° flexion angles respectively. Because of the negative initial strains of the PCL and femoral posterior translation, the PCL bundles were always slack without tensile forces (Figs. 8(i) and 8(j)). Compared with the CTKI, the STKI model showed much smaller collateral ligament forces. The patellar ligaments were also less stretched with smaller forces produced. The ACL was only in tension before 15° knee flexion.

Fig. 8

4. Discussion

This study aimed to simulate a CTKI using a dynamic FE model and considering the close-to-physiological muscle and ankle joint forces. The femoral external rotation and posterior translation of the CTKI with both cruciate ligaments retained were in good agreement with that of healthy knee measured by Murakami et al.[31] and other tibiofemoral motion ranges and patterns were also consistent with previous results from the literature[35, 36].

In contrast, the STKI in this study showed limited femoral external rotation during squatting, which was generally consistent with the results of another referenced STKI design[37] shown in Fig. 6(a). Some variations in the medial-lateral direction in the results from the STKI design in Fig. 6(c) were due to its symmetric structure. Its exponential increase in adduction rotation in Fig. 6(d) may show smaller collateral ligaments elongations and forces in the model, which consequently induced much smaller tibiofemoral compressive forces (Fig. 7). Smaller femoral superior translation in the STKI model (Fig. 6(e)) was mainly due to the revolute radius of the posterior condyles in the STKI being smaller than those of the CTKI whose profile is an ellipse in the sagittal plane.

The STKI resulted in smaller forces than the CTKI after 58° knee flexion. This was mainly due to smaller collateral ligaments forces and shorter elongations as shown in Fig. 6. It also indicates the significance of designing femoral posterior condyles with appropriate radii. Since a large volume of the posterior condylar bone is removed and replaced with the STKI which has posterior condyles of smaller radius, the distance between the femoral rotational axis and the tibial plateau becomes shorter. This could further decrease the elongation and tensile forces of the collateral ligaments, finally reducing the tibiofemoral contact forces. For the CTKI preliminary design in this study, because the femoral implant geometry was based on patient specific bone anatomy, only the shape or placement of the tibial component could be adjusted to create laxity in the knee joint.

Apart from the tibiofemoral forces, ligaments also affected the tibiofemoral motion of the CTKI model. As shown in Fig. 6(b), due to the tensile effect of the ACL, the femoral component could only gradually slide backwards in relation to the tibial counterpart, in the meantime, interacting with the tibial bearing surface in the

medial-lateral direction. However, for the ACL deficient models, the femoral component rapidly moved backwards by 10 mm in the first 5° knee flexion. The ACL is significant for the CTKI for maintaining knee stability during squatting in this study. The elongation variations of the ACL in the CTKI were generally consistent with the results of literature[38–40, 34]. Although the PCL does not contribute to the knee squat motion due to its negative initial pre-strain and the femoral posterior translation during squat, it is still important for other activities such as walking and stair-climbing in leg sway phase.

The fluctuations in the simulated results in this paper were probably caused by the lack of adduction-abduction moments in ankle and hip joints. The adduction-abduction moments could be applied on FE models in the future when the control algorithm is developed for balancing muscle forces with hip and ankle joint loads.

The FE model in this study and the Oxford and Kansas rigs can both be used to perform a squatting motion to assess the performances of total knee implants. However, it is very difficult to compare results directly due to the differences in structures and boundary conditions. Firstly, the translational degrees of freedom (DOFs) of the hip joint were constrained in the FE model, while the translational DOFs of the ankle joint were constrained in the Oxford[17-19] and Kansas[10-14] knee rigs. Secondly, twenty-three lower limb muscles including hamstrings and tibialis anterior muscles were simulated in the FE model with specific locations of muscle insertions, while only quadriceps were considered and simplified as an elastic strap driven by a servomotor in the Oxford and Kansas knee rigs. Thirdly, time-varying and vertical ankle joint loads were applied to the FE model in this study for considering the effect of ground reaction forces during the squatting motion. The ankle joint forces were calculated from the experimentally measured ground reaction forces using the reaction force algorithm in OpenSim software. In both the Oxford and Kansas knee rigs, on the other hand, the ground reaction forces as well as many muscles across the knee that in practice impact the natural knee joint forces were excluded. In the Oxford knee rig[17], only the quadriceps force and the vertically moving hip sled were used to reproduce the knee motion. For the Kansas knee rig[10, 13], loads were supplemented on the ankle joint DOFs of internal-external rotation, flexion-extension rotation and medial-lateral translation and a constant and small vertical force (200 N) was maintained on the assumed hip joint during the squatting motion. The quadriceps and hip vertical actuator were controlled in this knee rig to reproduce the desired tibiofemoral motions and forces. All these differences in structures and boundary conditions between the FE model of this study and the other two rigs make the comparisons of both kinematic and kinetic results difficult.

There are limitations in the musculoskeletal model in this paper. Neither patellar ligament nor collateral

ligaments were considered, because ligament structure is regarded as an external element in OpenSim. Its passive stretching during the motion could result in larger calculated joint reaction forces and muscle forces. In order to avoid introducing too many variables and in the context of lack of patient-specific muscle parameters, the generic musculoskeletal model 2392 with default muscle parameter setting was used for scaling. This would inevitably produce a certain amount of error. The measured data from the 4th Grand Challenge Competition to Predict In Vivo Knee Loads[24] were not used for comparing and validating the simulated tibiofemoral compressive forces, because the equations for converting measured data to tibiofemoral compressive forces have been validated only for gait motion.[41] The instrumented implant articulation does not match that of TKI models either.

5. Conclusion

A dynamic FE model was successfully created to compare a proposed anatomic CTKI with one off-the-shelf STKI. Different from the traditional knee simulators, the dynamic FE model in this study incorporated close-to-physiological muscle and ankle joint forces, which could make the computer simulations much closer to the actual physical and physiological environment. The CTKI design with both cruciate ligaments retained was simulated and the results showed that the knee could move naturally. However, improvement in the CTKI is still needed to reduce the large tibiofemoral compressive force after 50° knee flexion.

Acknowledgements

We would like to thank Dr Fiona Berryman for help with reviewing and proofreading. We also thank the Department of Engineering and Product Design, University of Sussex for financial support and Professor B.J. Fregly and his colleagues for providing publicly accessible data.

Competing interests: None declared

Funding: The Department of Engineering and Design, University of Sussex

Ethical approval: Not required

Appendix: Generating a customised knee implant

a) Modelling the femoral component

Layer scanning (Fig. A1) was adopted to capture the main features of the condyles and the trochlear groove. It was performed in the sequence shown in Fig. A1. For the posterior condyles, two boundary nodes, one peak nodes and two mid-nodes between the peak and boundary nodes were selected in each scanned layer. Based on

the coordinates of these nodes, key points (KPs) were then created. The same method was applied to the remaining part of the condyles with two boundary nodes, two peak nodes, one trough node and four mid-nodes in each layer. Although the created KPs were connected in the transverse and longitudinal directions using cubic spline interpolation to ensure the continuity and smoothness of the curves, the changing rate of surface curvatures of two adjacent areas was not continuous, which resulted in rough surfaces. Therefore, a least squares method of curve fitting was used to solve the issue of irregular changing of curvatures of longitudinal curves.

Fig. A1

Several fitting curves (circle, sphere, square curve, cubic curve) were explored, but the ellipse curve fitting was found to best fit the envelope of the sagittal sections of the condyle. Equations for the least squares method used to solve the expression function for the elliptical curves are shown below (Eqs. (1) to (5)).

$$\mathcal{E}_{yy} = \sum_{ii=0}^{mm} \left(xx_{ii}^2 + BBxx_{ii}yy_{ii} + CCyy_{ii}^2 + DDxx_{ii} + EEyy_{ii} + FF \right)^2 \quad (1)$$

$$xx_0^2 + BBxx_0yy_0 + CCyy_0^2 + DDxx_0 + EEyy_0 + FF = 0 \quad (2)$$

$$2xx_0 + BB(yy_0 + xx_0yy_0') + 2CCyy_0yy_0' + DD + EEyy_0' = 0 \quad (3)$$

$$xx_{mm}^2 + BBxx_{mm}yy_{mm} + CCyy_{mm}^2 + DDxx_{mm} + EEyy_{mm} + FF = 0 \quad (4)$$

$$\partial\partial\mathcal{E}/\partial\partial BB = \partial\partial\mathcal{E}/\partial\partial CC = \partial\partial\mathcal{E}/\partial\partial DD = \partial\partial\mathcal{E}/\partial\partial EE = \partial\partial\mathcal{E}/\partial\partial FF = 0 \quad (5)$$

$\mathcal{E}$ is the sum of the squares of the distances between points (xx_{ii}, yy_{ii}) to the curve: $xx^2 + BBxxyy + CCyy^2 + DDxx + EEyy + FF = 0$ in a plane which is determined by the KPs that need curve fitting in the longitudinal direction. To minimise $\mathcal{E}$, based on the extremum principle, Eq. (5) needs to be satisfied. Combining the boundary conditions and the Gaussian elimination method, the unknown parameter vector ($BBCCDDEEFF$) can be solved. The surfaces and volumes of the femoral component generated are shown in different views in Fig. 1a.

b) Modelling the tibial component

The natural tibial plateau consists of crescent-shaped menisci and articular surfaces, which makes the tibial bearing surfaces look like two different concave surfaces. Due to the lack of menisci images in the CT scans, the tibial bearing surfaces were initially assumed to have two different concave surfaces. The radii of their curvatures were designed to be larger than those of the femoral component, which would enable the femoral component to

move smoothly on the tibial counterpart. The lowest point on each condyle could be determined and was always located on the middle condylar curve in the longitudinal direction which was also the longest contour curve in each condyle of the femoral component. Because the aforementioned condylar curve consists of several spline curves with discrete KPs on two oblique planes, the KPs on the posterior and bottom condyle were selected and projected onto a fitting plane determined by three average points of those selected KPs. Lastly, a least squares elliptical fitting equation (Eq. (6)) was used to obtain an ellipse which will be the closest to those projected KPs (Fig. A2 (a)).

Fig. A2

$$\mathcal{E} = \sum_{ii=1}^{nn} xx_{ii}^2 + BByy_{ii}^2 + CCxx_{ii} + DDyy_{ii} + EE^2 \tag{6}$$

Since boundary conditions $xx_0 = yy_0 = yy'_0 = 0$ are known, these are substituted into Eq. (6) and its corresponding derivative equations are shown in Eq. (7):

$$\begin{aligned} 2xx_0 + 2BByy_0yy'_0 + CC + DDyy'_0 &= 0 \\ xx_0^2 + BByy_0^2 + CCxx_0 + DDyy_0 + EE &= 0 \end{aligned} \tag{7}$$

$CC = EE = 0$ is then obtained and Eq. (6) istransformed:

$$\mathcal{E} = \sum_{ii=1}^{nn} xx_{ii}^2 + BByy_{ii}^2 + DDyy_{ii}^2 \tag{8}$$

$$\partial\partial\mathcal{E}/\partial\partial BB = 2\sum_{ii=1}^{nn} xx_{ii}^2 + BByy_{ii}^2 + DDyy_{ii} yy_{ii}^2 = 0 \tag{9}$$

$$\partial\partial\mathcal{E}/\partial\partial DD = 2\sum_{ii=1}^{nn} xx_{ii}^2 + BByy_{ii}^2 + DDyy_{ii} yy_{ii} = 0 \tag{10}$$

Once the coefficients B and D have been solved through Eqs. (9) and (10) by substituting the coefficients C and E, the fitting elliptical equation can be obtained as Eq. (11):

$$xx^2/(DD^2/4BB) + (yy + DD/2BB)^2/(DD^2/4BB^2) = 1 \tag{11}$$

The long axis of the elliptical curve is $aa_{eellllliieeeeee} = \sqrt{D^2/4BB}$. While keeping the short axis constant, increasing $aa_{eellllliieeeeee}$ to a new $aa_{eellllliieeeeee\_nneenn}$ would increase the radius of curvature of the ellipse, making the cutting guide track and its counterpart tibial bearing surface flatter. In this study, the relationship $aa_{eellllliieeeeee\_nneenn} = 4aa_{eellllliieeeeee}$ was assumed.

Once the tibial cutting guidance track was obtained, the cutting contour could be created. As can be seen in Fig. A2 (b), the transverse condylar curve can be divided into two segments. Because the curvatures of the two segments are quite different, the two KPs, medial and lateral ones on each segment, were selected along with the lowest KP for quadratic least square fitting (red dot curve in Fig. A2 (b)). Through adjusting the coefficients of the equations, a larger radius of curvature for each fitting curve (blue solid curve in Fig. A2 (b)) can be created. The KP in the origin of the working plane coincides with the lowest KP on the femoral condyle. The tangent conditions can ensure the two quadratic curves connect smoothly and are tangential to the femoral condyle. The tibial bearing surface was then built using those two quadratic curves as the contour and the elliptical curve as the cutting guide track. In this study, the medial quadratic coefficients: $aa_{1\_nneenn} = aa_1/4$, lateral: $aa_{2\_nneenn} = aa_2/6$, were assumed in both condyles.

References

1. Noble PC, Gordon MJ, Weiss JM, et al. Does Total Knee Replacement Restore Normal Knee Function?: *Clinical Orthopaedics and Related Research* 2005; 157–165.
2. Bourne RB, Chesworth BM, Davis AM, et al. Patient Satisfaction after Total Knee Arthroplasty: Who is Satisfied and Who is Not? *Clinical Orthopaedics and Related Research* 2010; 468: 57–63.
3. Mahoney OM, Kinsey T. Overhang of the Femoral Component in Total Knee Arthroplasty: Risk Factors and Clinical Consequences: *The Journal of Bone and Joint Surgery-American Volume* 2010; 92: 1115–1121.
4. Ali A, Sundberg M, Robertsson O, et al. Dissatisfied patients after total knee arthroplasty: A registry study involving 114 patients with 8–13 years of follow-up. *Acta Orthopaedica* 2014; 85: 229–233.
5. Nam D, Nunley RM, Barrack RL. Patient dissatisfaction following total knee replacement: a growing concern? *The Bone & Joint Journal* 2014; 96-B: 96–100.
6. Bonnefoy-Mazure A, Armand S, Sagawa Junior Y, et al. Evolution of knee kinematics three months after total knee replacement. *Gait & Posture* 2015; 41: 624–629.
7. Rahman J, Tang Q, Monda M, Miles J, McCarthy I. Gait assessment as a functional outcome measure in total knee arthroplasty: a cross-sectional study. *BMC Musculoskeletal Disorders* 2015; 16:66.
8. Walker PS, Lowry MT, Kumar A. The Effect of Geometric Variations in Posterior-stabilized Knee Designs on Motion Characteristics Measured in a Knee Loading Machine. *Clinical Orthopaedics and Related Research* 2014; 472: 238–247.

9. Patil S, Bunn A, Bugbee WD, et al. Patient-specific implants with custom cutting blocks better approximate natural knee kinematics than standard TKA without custom cutting blocks. *The Knee* 2015; 22: 624–629.

10. Baldwin MA, Clary CW, Fitzpatrick CK, et al. Dynamic finite element knee simulation for evaluation of knee replacement mechanics. *Journal of Biomechanics* 2012; 45: 474–483.

11. Baldwin MA, Clary C, Maletsky LP, et al. Verification of predicted specimen-specific natural and implanted patellofemoral kinematics during simulated deep knee bend. *Journal of Biomechanics* 2009; 42: 2341–2348.

12. Bloemker KH, Guess TM, Maletsky LP, Dodd K. Computational knee ligament modeling using experimentally determined zero-load lengths. *The Open Biomedical Engineering Journal* 2012; 6; 33–41

13. Guess TM, Maletsky LP. Computational Modeling of a Dynamic Knee Simulator for Reproduction of Knee Loading. *Journal of Biomechanical Engineering* 2005; 127: 1216.

14. Guess TM, Maletsky LP. Computational modeling of a dynamic knee simulator for prediction of joint loading. *2003 Summer Bioengineering Conference*. Florida, 2003.

15. Hacker SP, Ignatius A, Dürselen L. The influence of the test setup on knee joint kinematics – A meta-analysis of tibial rotation. *Journal of Biomechanics* 2016; 49: 2982–2988.

16. Verstraete MA, Victor J. Possibilities and limitations of novel in-vitro knee simulator. *Journal of Biomechanics* 2015; 48: 3377–3382.

17. Varadarajan KM, Harry RE, Johnson T, et al. Can in vitro systems capture the characteristic differences between the flexion–extension kinematics of the healthy and TKA knee? *Medical Engineering & Physics* 2009; 31: 899–906.

18. Bourne R, Goodfellow JW, O'Connor JJ. A functional analysis of various knee arthroplasties. In: *Transactions of the 24th Annual Orthopaedic Research Society*. Dallas, 1978.

19. Zavatsky AB. A kinematic-freedom analysis of a flexed-knee-stance testing rig. *Journal of Biomechanics* 1997; 30: 277–280.

20. Maletsky LP, Hillberry BM. Simulating Dynamic Activities Using a Five-Axis Knee Simulator. *Journal of Biomechanical Engineering* 2005; 127: 123.

21. Maletsky LP, Hillberry BM. Loading Evaluation of Knee Joint During Walking Using the Next Generation Knee Simulator. *Advances in Bioengineering* 2000; 48: 91–92.

22. Escamilla RF. Knee biomechanics of the dynamic squat exercise: *Medicine and Science in Sports and Exercise* 2001; 127–141.

23. Fedorov A, Beichel R, Kalpathy-Cramer J, et al. 3D Slicer as an image computing platform for the Quantitative Imaging Network. *Magnetic Resonance Imaging* 2012; 30: 1323–1341.

24. Fregly BJ, Besier TF, Lloyd DG, et al. Grand challenge competition to predict in vivo knee loads. *Journal of Orthopaedic Research* 2012; 30: 503–513.

25. Shi J. Finite element analysis of total knee replacement considering gait cycle load and malalignment. University of Wolverhampton 2007, http://wlv.openrepository.com/wlv/handle/2436/14404.

26. Dai Y, Scuderi GR, Penninger C, et al. Increased shape and size offerings of femoral components improve fit during total knee arthroplasty. *Knee Surgery, Sports Traumatology, Arthroscopy* 2014; 22: 2931–2940.

27. Buschmann J, Meier Bürgisser G. Biomechanical properties of tendons and ligaments in humans and animals. In: *Biomechanics of Tendons and Ligaments*. Elsevier, pp. 31–61.

28. Beidokhti HN, Janssen D, van de Groes S, et al. The influence of ligament modelling strategies on the predictive capability of finite element models of the human knee joint. *Journal of Biomechanics* 2017; 65: 1–11.

29. Blankevoort L, Huiskes R. Ligament-Bone Interaction in a Three-Dimensional Model of the Knee. *Journal of Biomechanical Engineering* 1991; 113: 263.

30. Butler D, Kay M, Stouffer D. Comparison of material properties in fascicle-bone units from human patellar tendon and knee ligaments. *Journal of Biomechanics* 1986; 19(6): 425–32.

31. Murakami K, Hamai S, Okazaki K, et al. In vivo kinematics of healthy male knees during squat and golf swing using image-matching techniques. *The Knee* 2016; 23: 221–226.

32. Stylianou AP, Guess TM, Kia M. Multibody Muscle Driven Model of an Instrumented Prosthetic Knee During Squat and Toe Rise Motions. *Journal of Biomechanical Engineering* 2013; 135: 041008.

33. Taylor WR, Schütz P, Bergmann G, et al. A comprehensive assessment of the musculoskeletal system: The CAMS-Knee data set. *Journal of Biomechanics* 2017; 65: 32–39.

34. Bersini S, Sansone V, Frigo CA. A dynamic multibody model of the physiological knee to predict internal loads during movement in gravitational field. *Computer Methods in Biomechanics and Biomedical Engineering* 2016; 19: 571–579.

35. Belvedere C, Leardini A, Giannini S, et al. Does medio-lateral motion occur in the normal knee? An in-vitro study in passive motion. *Journal of Biomechanics* 2011; 44: 877–884.

36. Nordin M, Frankel VH. *Basic Biomechanics of the Musculoskeletal System*. 3rd ed. Lippincott Williams & Wilkins, 2001.

37. Murakami K, Hamai S, Okazaki K, et al. Knee kinematics in bi-cruciate stabilized total knee arthroplasty during squatting and stair-climbing activities. *Journal of Orthopaedics* 2018; 15: 650–654.

38. Beynnon BD, Fleming BC. Anterior cruciate ligament strain in-vivo: A review of previous work. *Journal of Biomechanics* 1998; 31: 519–525.

39. Li G, DeFrate LE, Sun H, et al. In Vivo Elongation of the Anterior Cruciate Ligament and Posterior Cruciate Ligament during Knee Flexion. *The American Journal of Sports Medicine* 2004; 32: 1415–1420.

40. Hosseini A, Gill TJ, Li G. In vivo anterior cruciate ligament elongation in response to axial tibial loads. *Journal of Orthopaedic Science* 2009; 14: 298–306.

41. Zhao D, Banks SA, D'Lima DD, et al. In vivo medial and lateral tibial loads during dynamic and high flexion activities. *Journal of Orthopaedic Research* 2007; 25: 593–602.

Fig. 1(a) Customised femoral implant; (b) scaled off-the-shelf femoral implant of DePuy PFC Sigma system [25]

Fig. 2(a) Tibial insert model of CTKI and the tibial tray of 3 mm thickness (red); (b) Scaled DePuy PFC Sigma system tibial implant [25]

Fig. 3 (a) Process of patient-specific loads calculation for squatting motion; (b) hip flexion and pelvis vertical translation; (c) ankle joint reaction loads (superior-inferior force, medial-lateral force, anterior-posterior force, flexion-extension moment and internal-external moment); (d) and (e) muscle forces of the left lower limb

Fig. 4 Dynamic finite element model (a) joints and boundary conditions; (b) musculotendons and ligaments (aMCL, aLCL: anterior bundles of medial and lateral collateral ligaments; mMCL, mLCL: middle bundles of medial and lateral collateral ligaments; pMCL, pLCL: posterior bundles of medial and lateral collateral ligaments); (c) cruciate ligaments (without corresponding design features in the tibial insert); (d) quadriceps muscles

Fig. 5 Schematic representation of connection definitions

Fig. 6 Tibiofemoral relative motions: (a) and (b) comparisons of simulated external rotation and anterior translation with reported five healthy male knees which are shown in cyan triangle lines and implanted knees with bi-cruciate stabilized (BCS) design in black dot line. (c)~(e) medial-lateral translation, adduction-abduction rotation and superior-inferior translation. Shaded areas in red, green and blue are simulated results under different pre-strains of collateral ligaments: -50%, -20%, -10%, 10%, 20%, 50% of the reference strain in Table 2.

Fig. 7 Tibiofemoral (TF) compressive forces: (a) total condylar compressive forces including comparisons with other research findings; (b) medial and (c) lateral tibiofemoral contact forces. Shaded areas in red, green and blue were calculated and plotted under different pre-strains of collateral ligaments: -50%, -20%, -10%, 10%, 20%, 50% relative to the reference strain in Table 2.

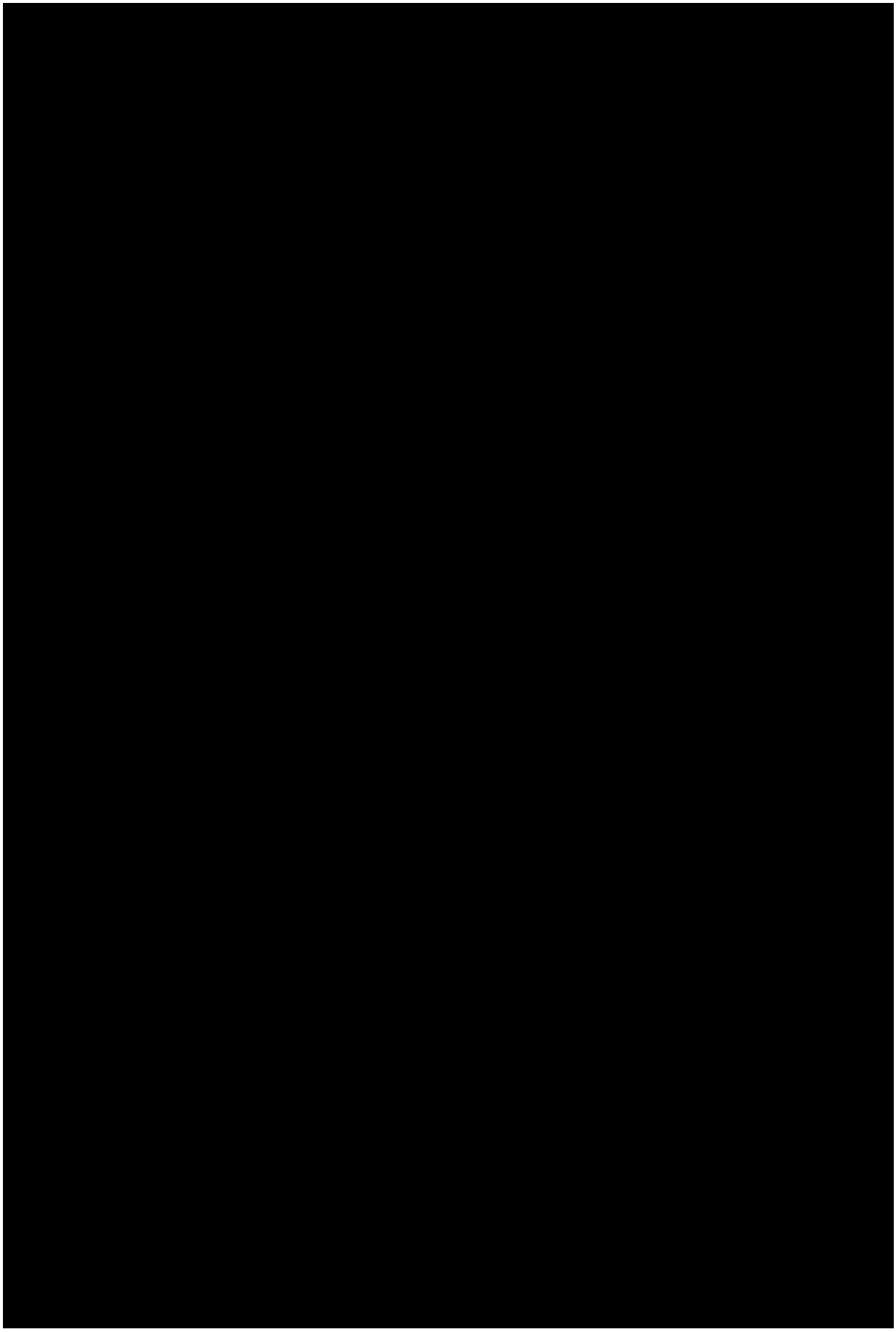

Fig. 8 Tensile forces of (a) medial collateral ligaments (MCLs), (c) lateral collateral ligaments (LCLs), (e) patellar

ligaments (PLs), (g) anterior cruciate ligaments (ACLs), (i) posterior cruciate ligaments (PCLs) and the elongations of (b) MCL, (d) LCL, (f) PL, (h) ACL, (j) PCL under three scenarios: retained ACL and PCL, removed ACL and PCL and only removed ACL for the CTKI, and one scenario of retained cruciate ligaments for the STKI

Fig. A1 Sequence of layer scanning. a, d, e, f and h for transverse scanning; b, c and g for rotational scanning

Fig. A2 Modelling of tibial bearing surface (a) cutting guide curve; (b) transverse contour

Table 1 Subject-specific left leg masses and mass centres scaled from the generic model

	Mass (Kg)	Mass centre (m)	Inertia xx ($kg \cdot m^2$)	Inertia yy ($kg \cdot m^2$)	Inertia zz ($kg \cdot m^2$)
Femur_l	8.253930	(0 -0.173507 0) in Hip_l joint coordinate system	0.123774	0.032446	0.130522
Tibia_l	3.289983	(0 -0.188756 0) in Knee_l joint coordinate system	0.045714	0.004626	0.046349

Table 2 Collateral ligament and cruciate ligament stiffness parameters and reference strains [28, 29]

	aLCL	mLCL	pLCL	aMCL	mMCL	pMCL	aPCL	pPCL	aACL	pACL
Ligament stiffness parameter (N)	2000	2000	2000	2750	2750	2750	9000	9000	5000	5000
Reference strain/ initial spring strain	-0.25	-0.05	0.08	0.04	0.04	0.03	-0.24	-0.03	0.06	0.1

Table 3 Material property setting of total knee implant components [25]

	Elasticity modulus (MPa)	Poisson's ratio	Coefficient of friction	Density (kg/m^3)
UHMWPE	1016	0.46	0.04	0.945×10^3
Cobalt-Chrome alloy	193000	0.29	0.05	8.5×10^3
Titanium alloy	110000	0.33		4.4×10^3
Cortical bone	17580	0.3	0.8	1.85×10^3